ESA Climate Change Initiative

Antarctica Ice Sheet CCI+

Option 3 - Timeseries of ice discharge and IOM mass balance for the East and West Antarctic Ice Sheets from Sentinel-1

End-to-End Uncertainty Budget (E3UB)

Deliverable ID: O3-D2.3

Lead Author: Jan Wuite
ENVEO Environmental Earth Observation GmbH (ENVEO), Innsbruck, Austria

Technical Officer: Simon Pinnock
ESA ECSAT, Harwell, United Kingdom

Consortium: ENVEO Environmental Earth Observation GmbH (ENVEO)
Northumbria University (NU), Newcastle-upon-Tyne, United Kingdom
Technical University of Denmark-DTU Space GDK (DTU), Denmark
Science and Technology AS (S&T)

Signatures page

Compiled by	Jan Wuite Lead Author, ENVEO	
Approved by	Andrew Shepherd, Project Manager, NU	
Approved by	Thomas Nagler Science Leader, ENVEO	
Approved by	Simon Pinnock ESA Technical Officer	

Table of Contents

Change Log

Issue	Author	Affected Section	Change	Date
1.0	Jan Wuite	All	First Version	7/09/2025
1.1	Jan Wuite	2.4	Comments addressed	27/10/2025

Acronyms and Abbreviations

Acronyms	**Explanation**
AIS	Antarctic Ice Sheet
CCI	Climate Change Initiative
CCN	Contract Change Notice
DTU	Technical University of Denmark
EAIS	East Antarctic Ice Sheet
ECV	Essential Climate Variable
ENVEO	Environmental Earth Observation
ENVISAT	Environmental Satellite
ERS-1/2	European Remote Sensing satellite 1 & 2
ESA	European Space Agency
GLL	Grounding Line Location
IMBIE	Ice sheet Mass Balance Inter-comparison Exercise
InSAR	Interferometric synthetic-aperture radar
IOM	Input-Output Method
IV	Ice Velocity
MEaSUREs	Making Earth System Data Records for Use in Research Environments
MFID	Mass Flux Ice Discharge
NU	Northumbria University
S1	Sentinel-1
S&T	Science and Technology AS
SAR	Synthetic Aperture Radar
SEC	Surface Elevation Change
SLC	single look complex
SMB	Surface Mass Balance
TCM	Tidal Correction Module
TDX	TanDEM-X
TSX	TerraSAR-X
WAIS	West Antarctic Ice Sheet
WP	Work Package

1 Introduction

1.1 Purpose and Scope

This document contains the End-to-end Uncertainty Budget (E3UB, O3-D2.2) for Option-3 as part of the Antarctic Ice Sheet CCI+ project Phase 2, in accordance with contract and proposal [AD1 and AD2]. The E3UB is delivered as part of WP3200 - Algorithm Development and Uncertainty Estimation – and describes the error characteristics of the algorithms used and in development in the project for retrieving ice velocity (IV), mass flux ice discharge (MFID) and IOM mass budget (MB). The document describes the best current understanding of the sources of errors and uncertainties, considering errors induced by sensors, models, corrections, technical developments, and continued validation/inter-comparison efforts. The physical and technical basis of the algorithms for homogenised time series of ice velocity and ice discharge for the Antarctic Peninsula is reported in the Algorithm Theoretical Basis Document (ATBD, O3-D2.2).

1.2 Document Structure

This document is structured as follows:

- Chapter 1 contains an introduction to the document,
- Chapter 2 describes the End-to-end Uncertainty Budget for IV,
- Chapter 3 describes the End-to-end Uncertainty Budget for MFID,
- Chapter 4 describes the End-to-end Uncertainty Budget for MB,
- Chapter 5 lists the references

1.3 Applicable and Reference Documents

Table 1.1: List of Applicable Documents

No	Doc. Id	Doc. Title	Date	Version
AD1	ESA/Contract No. 4000143397/23/I-NB CCI+ PHASE 2 – AIS	CCI+ PHASE 2 - NEW R&D ON CCI ECVS for AIS CCI	13.02.2024	1
AD2	ENVEO-NU-DTU-SNT-AISCCI+-P2-Option3-MFID-001_v06	Technical proposal for Option 3	01.12.2023	

Table 1.2: List of Reference Documents

No	Doc. Id	Doc. Title	Date	Version
RD1	ENVEO-NU-DTU-SNT-AISCCI+-P2-Option3-D2.1_ATBD	Algorithm Theoretical Basis Document (ATBD) for AIS CCI+ P2 Option-3	2025.09.31	V1.0
RD2	ST-UL-ESA-AISCCI+-E3UB-001	End-to-end Uncertainty Budget (E3UB) for Antarctic Ice Sheet CCI+ Phase 1	2020.05.20	v1.0
RD3	ST-DTU-ESA-GISCCI+-E3UB-001-v1.1	End-to-end Uncertainty Budget (E3UB) for Greenland Ice Sheet CCI+ Phase 1	2020.05.05	v1.1
RD4	ST-UL-ESA-AISCCI+-PUG-001	Product User Guide (PUG) for Antarctic Ice Sheet CCI+ Phase 1	2021.04.30	v1.0

2 Ice Velocity

2.1 Introduction

The ice velocity (IV) maps that are generated in this project are derived from multi-sensor and multi-temporal synthetic aperture radar (SAR) data, mainly using offset tracking (OT). The development and production of IV maps in this project build on the achievements of previous projects, including Antarctic Ice Sheet CCI and Greenland Ice Sheet CCI. Sources of errors and uncertainties, both internal (i.e. algorithm dependent) and external, as well as methods for accuracy determination and the accuracy to be reported, are discussed in detail in [RD1, RD2, RD3] and summarised here.

2.2 Sources of error

Offset-based IV retrieval methods are sensitive to all factors which may contribute to image misalignment between two acquisitions in both the slant-range and azimuth dimensions. The error sources include orbital and topographic uncertainties, tropospheric and ionospheric signal delay and decorrelation due to phenomena, like strong velocity gradients, temporal variations of the properties of the scattering volume and different viewing geometries at the image acquisition times. The topographic component mainly impacts the slant-range offset measurements, whereas the dominating atmospheric error component is due to ionospheric propagation and causes spatially varying mis-registration in the azimuth dimension. A calibration procedure, exploiting a set of GCPs or external IV maps, is required in general to compensate for long wavelength error trends.

2.3 Methodology for determination of error and uncertainty

The error prediction framework described in (Mohr and Merryman Boncori, 2008) is applied to derive estimates of the error standard deviation of slant-range and azimuth velocity measurements. The framework was originally proposed for InSAR techniques, but has been successfully extended to offset-tracking techniques. The input to the framework consists in the location of the GCPs used for velocity calibration, and in models for the covariance function (or equivalently the structure function) of all error sources, including atmospheric propagation. For a mathematical formulation, the reader is referred to (Mohr and Merryman Boncori, 2008). The slant-range and azimuth error standard deviations are propagated to the output Cartesian velocity components in the velocity inversion. In areas where multiple tracks are combined, the error estimates are used to do a weighted average of the displacement measurements, and the error estimate of the output product is updated to reflect this.

In addition, stable terrain tests are carried out. This internal assessment method analyses stable ground where no displacement is expected. This gives a good overall indication of the bias introduced by the end-to-end velocity retrieval, including co-registration of images, velocity retrieval, etc. After performing the matching for the entire region covered by the image pair, the results for the ice-covered (moving) area will be separated from the ice-free (stable) ground. The masking is done using external information, e.g. polygons of the ice-free stable land areas. Buffers around the glacier polygon are applied before the extraction of stable ground for statistical calculation (bias, RMSE).

2.4 Error and uncertainty documentation

The output from the error prediction described in the previous section is a pixelwise estimate of the standard deviation. Each generated map will be accompanied by its uncertainty, which is calculated from the standard deviation of all valid observations during the month/year on a per-pixel basis for both (horizontal) velocity components. The uncertainty is also provided as a map, in the same geometry as the associated velocity map, providing a measure of uncertainty on a per-pixel basis (Figure 2.1). We do not consider it as an error map, but rather an uncertainty map,since the standard deviation for each pixel also captures real sub-monthly/annual velocity fluctuations. The uncertainty map provides a measure of confidence of the calculated mean and is only provided for pixels with more than one valid observation. The uncertainty map, however, is not derived from the error budget of the image matching or the strength of the correlation peak itself.

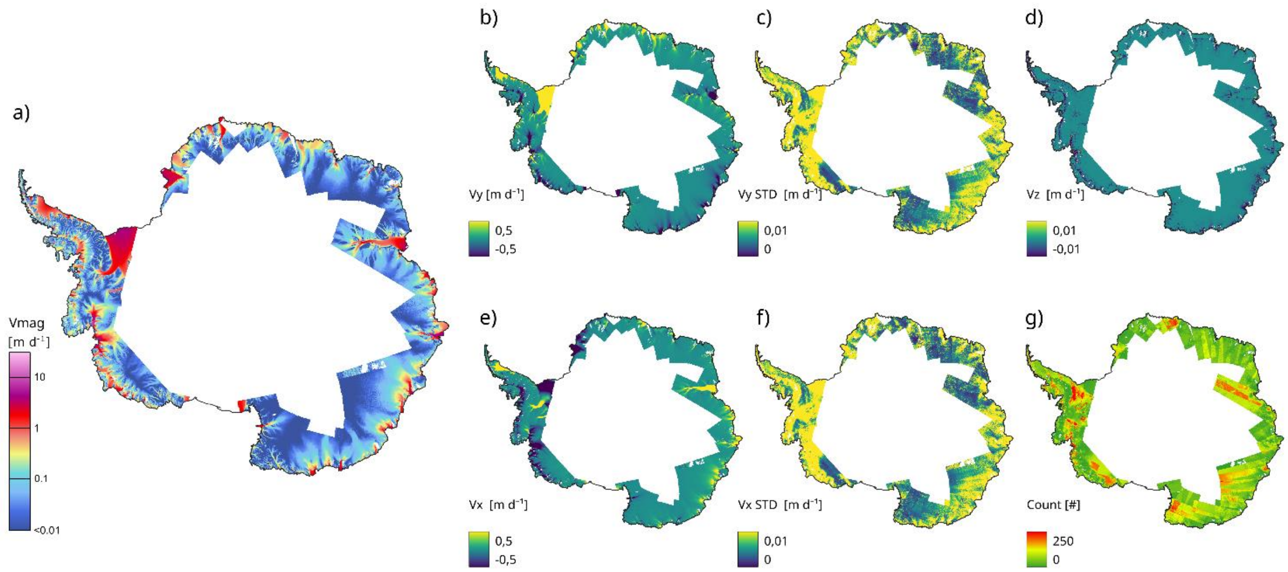

Figure 2.1: Annual ice velocity map for Antarctica 2021/22, showing a) velocity magnitude; b) northing component of velocity; c) std of northing component; d) vertical component (derived from DEM); e) easting component of velocity; f) std of easting component; g) valid measurement count.

2.5 Guideline for using the product

The IV product is distributed in NetCDF files following the conventions described in the Product User Guide (PUG) [RD4]. The estimated error standard deviations are provided on the same grid as the ice velocity estimates in the variables:

- land_ice_surface_easting_velocity_std
- land_ice_surface_northing_velocity_std

3 Mass Flux Ice Discharge

3.1 Introduction

The mass flux/ice discharge or MFID constitutes the 'output' in the Input-Output Method (IOM). It is calculated from (time series of) ice velocity fields that are combined with ice thickness data at pre-defined flux gates near the grounding line or termini of marine outlet glaciers or ice streams. The solid ice discharge estimates rely on accurate ice thickness and velocity measurements. The uncertainty is therefore largely determined by the quality of these input data.

3.2 Sources of error

Error sources include the following:

- Velocity (see Chapter 2)
- Ice thickness

3.3 Methodology for determination of error and uncertainty

The error is quantified based on the uncertainties reported in the input data products, with consideration of their relative propagation into the final estimate, the distinction between random and systematic components, and the potential dependence among variables. The error of the mass flux δΦ across a flux gate is calculated with:

$$\delta\Phi = \sum_i \Phi_i \sqrt{\left(\frac{\delta H_i}{H_i}\right)^2 + \left(\frac{\delta v_i}{v_i}\right)^2}$$

where δH is the error of the ice thickness H in m and δv the error of the ice velocity magnitude v in m/d. As radar flight tracks are often incomplete, especially along fast-moving glaciers that flow through steep and/or narrow fjords, data gaps exist that need to be filled in. The ice bed models use an optimal approach to fill these gaps, but nevertheless, uncertainties can be significant, in particular for glaciers with few observations and/or a large imbalance (Figure 3.1). To minimise the uncertainty associated with thickness, flux gates are preferably selected along flight tracks. This means, however, that in some cases discharge estimates are based on flux gates that are situated some distance above the grounding line, hence requiring a correction for the unsurveyed area.

Changes in ice thickness at the grounding line affect the flux calculation to some degree, but the uncertainty associated with this is much smaller than the uncertainty of the ice thickness. Changes in ice thickness are accounted for by using monthly SEC fields derived from multi-mission satellite radar altimetry (Shepherd et al., 2019). The single-mission elevation change uncertainty was estimated as a combination of systematic and time-varying error sources. The systematic component represents effects such as unmodelled short-lived accumulation events or changes in snowpack properties and is defined by the standard error of the surface elevation rate of change (dz/dt) derived from the time series and was accumulated linearly with time, such that its contribution grew at each epoch. The time-varying component arises from factors like measurement noise and spatial sampling variability and is determined from the dispersion of pixel-level dz measurements at each epoch and, being temporally uncorrelated, was propagated in quadrature across all preceding epochs. These two terms were then summed in quadrature to yield the total single-mission uncertainty.

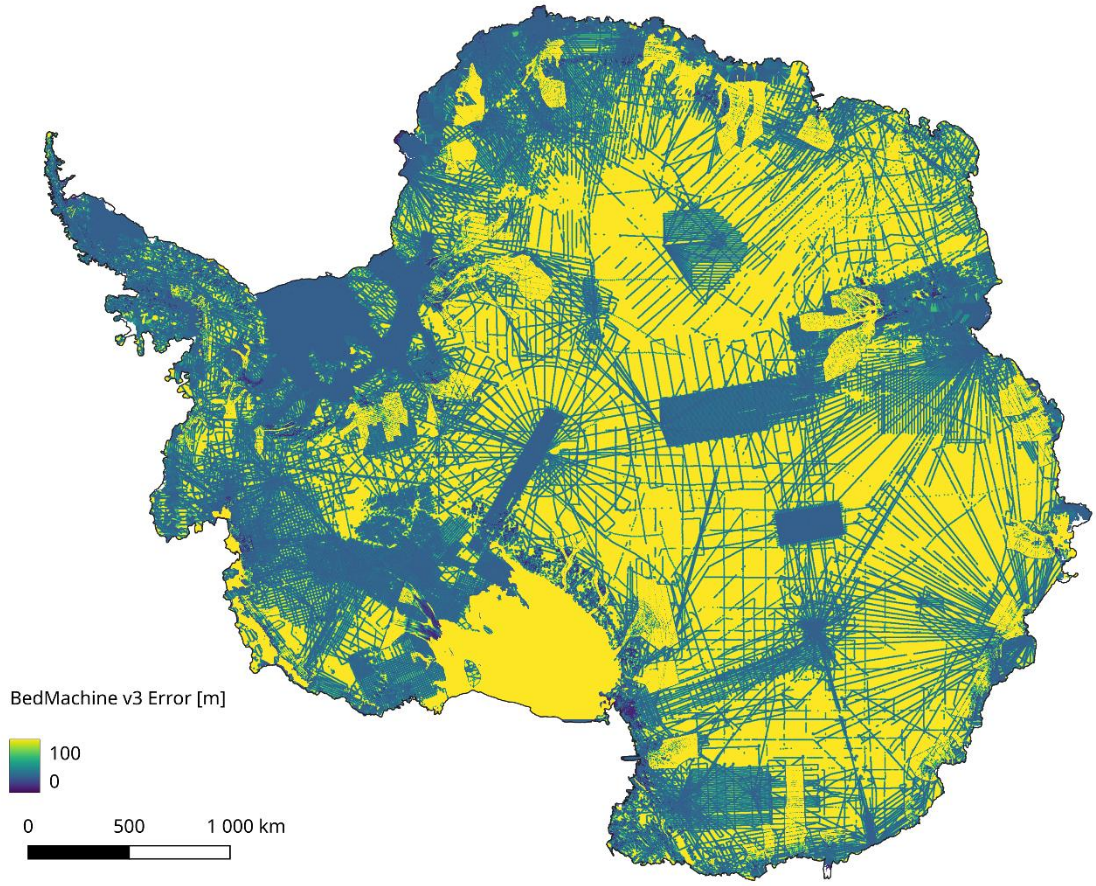

Figure 3.1: BedMachine Antarctica error (Morlighem et al., 2022).

The combined multi-mission uncertainty was estimated by additionally accounting for inter-satellite biasing errors, quantified as the standard deviation of differences between modelled elevations during mission overlap periods. This biasing uncertainty was set to zero for the first mission (ERS-1) and added in quadrature at each subsequent inter-mission boundary, before being combined in quadrature with the single-mission uncertainty to produce the total multi-mission uncertainty at each epoch. Finally, for the modelled monthly elevation change time series (ΔH), a quadratic function $\Delta H = at^2 + bt + c$ was fitted to the observations, with a, b, and c as the quadratic, linear, and intercept coefficients. Uncertainty in ΔH ($\Delta H\sigma$) was derived from the 95% confidence bounds on the coefficients ($a\sigma$, $b\sigma$, $c\sigma$) by computing the maximum and minimum possible elevation changes (ΔH_{max} and ΔH_{min}) from the preceding uncertainties and scaling the resulting error estimate by the ratio of the original observational frequency (140 days) to the fit sampling frequency (monthly), ensuring that the error did not artificially scale with sampling resolution (Davison et al., 2025).

3.4 Error and uncertainty documentation

The primary output data are solid ice discharge estimates for basins in EAIS and WAIS that drain into either the ocean or ice shelves fringing the coast (e.g. Ross, Ronne Filchner, Getz, Amery, Fimbul, Brunt). The discharge estimates are provided in CSV table format in Gigatons per year (Gt/Y), averaged for a specified time period along with their associated uncertainties (and graphically with error bars).

3.5 Guideline for using the product

The primary source of uncertainty is the ice thickness uncertainty, which is systematic and fixed in time. Therefore, aggregating discharge spatially or temporally will not reduce that uncertainty. To help minimise the error/uncertainty associated with ice thickness, flux gates used for discharge estimates are preferably selected along or near radar flight tracks.

Another source of error for discharge calculation arises from resampling of the grounding line to equally spaced points along that line. As illustrated in Figure 3.2 by extracting equally spaced points along the line geometry, the resulting actual distance between the points can be smaller. Since the distance between the points is directly used in the formula for calculating the mass flux as the width of the gate, an error is made if the actual distance differs from the intended distance. The sharper the edges of the original grounding line and the smaller the distance between the original vertices in comparison to the intended distance, the bigger the error that is introduced. Estimates of the final error and options to avoid this source of error are currently under investigation and will be included in the next version of the document.

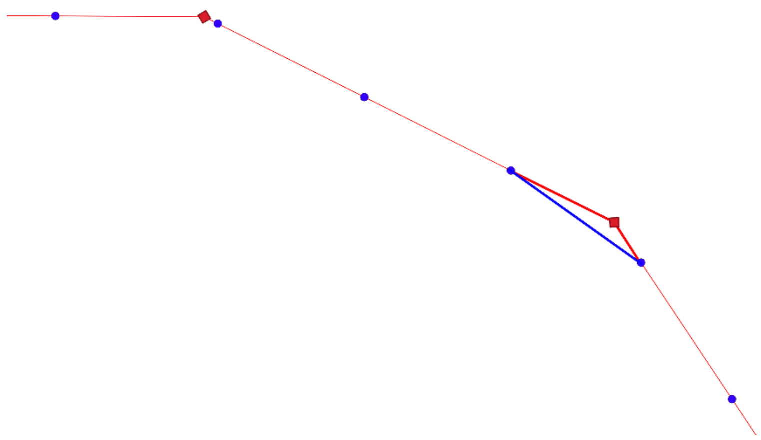

Figure 3.2: Example for equally spaced points along the grounding line. Red diamonds indicate the vertices of the original grounding line. Blue points indicate the calculated points along the original grounding line, with presumably equal distances between the points. The thick red line indicates the distance between the two neighbouring blue points, which agrees with the intended equal distance between all blue points. However, the thick blue line represents the real distance between the two points, which can be smaller than the intended distance.

Other sources of errors, which are random, do exist and can be reduced by aggregating results over large areas or times. We therefore use basin-wide discharge or regional discharge, and caution when examining individual glaciers. Similarly, annual or monthly averaged or summed results will have a higher signal-to-noise ratio than individual time steps.

Methods for handling data gaps in ice velocity and thickness, and handling erroneous ice thickness are discussed in detail in the Algorithm Theoretical Basis Document (ATBD) [RD1].

4 IOM Mass Budget

4.1 Introduction

The IOM Mass Budget or Mass Balance (MB) is calculated from the difference in ice discharge (D) and surface mass balance (SMB):

$$\text{Mass Budget (MB)} = \text{Surface Mass Balance (SMB)} - \text{Ice Discharge (D)}$$

- If SMB > D, the ice sheet gains mass (positive balance)
- If SMB < D, the ice sheet loses mass (negative balance)

The IOM MB is calculated for each month and every basin separately, and also combined to provide an ice sheet-wide estimate of mass balance. The uncertainty in the IOM method hence, arises from both the limitations of the SMB model and the uncertainty in the calculated ice discharge.

4.2 Sources of error

For this version of the report, we provide in this chapter a high-level overview of the types of errors associated with the IOM approach for quantifying Antarctic ice mass loss. In the next version of the report, these will be further detailed and quantified.

4.2.1 Errors in Surface Mass Balance

- Model uncertainty: SMB is usually derived from regional climate models (e.g., RACMO, MAR), which include uncertainties in precipitation, sublimation, melt, and refreezing.
- Forcing errors: Biases in atmospheric reanalysis products used to drive the regional models.
- Spatial/temporal resolution: Coarse resolution may smooth small-scale processes (e.g., orographic snowfall).
- Projection errors: The computation of SMB requires reprojecting the RACMO 2.3 raster to the coordinate reference system of the basin geometries to enable intersection analysis. This transformation is performed using GDAL, which relies on the raster's georeferencing parameters, including origin location, pixel size, and rotation terms. Consequently, even minor uncertainties in these parameters may affect the accuracy of the SMB estimates for individual basins.

4.2.2 Errors in Ice Discharge Estimates

- Ice velocity uncertainties: Derived from satellite InSAR, affected by resolution, temporal coverage, and noise.
- Thickness errors: Errors in ice thickness from radar surveys (elevation changes, sparse coverage, interpolation, radar penetration issues).
- Grounding line location: Misplacement of grounding lines alters flux gates.
- Tide and firn corrections: Affects elevation-to-thickness conversion.
- Interpolation and extrapolation: Sparse velocity/thickness data must often be interpolated across flux gates.

4.3 Methodology for determination of error and uncertainty

The methodology for the determination of the error and uncertainty in ice velocity and ice discharge is discussed in chapters 2 and 3. If we assume the uncertainties in SMB and discharge are independent, the combined uncertainty in the mass balance is obtained by propagation of independent errors using the square root of the sum of squares:

$$\sigma_{IOM\,MB} = \sqrt{\sigma_{SMB}^2 + \sigma_{MFID}^2}$$

The assumption of independence is common because SMB errors (climate model uncertainties) and discharge errors (velocity, thickness, grounding line) arise from different sources.

4.4 Error and uncertainty documentation

The IOM MB estimates are provided in CSV table format in Gigatons per year (Gt/Y) averaged for a specified time period, along with their associated uncertainties (and graphically with error bars).

4.5 Guideline for using the product

Currently, the analysis relies solely on a single SMB model, RACMO 2.3 (Van Wessem et al., 2014). The use of alternative SMB models, or combinations of multiple models, could yield different SMB estimates and associated uncertainties, reflecting variations in model physics, spatial resolution, and input forcing datasets (Mottram et al., 2021). Incorporating multiple SMB models would provide a more comprehensive assessment of model-dependent uncertainty, allowing for a better characterisation of the potential range of ice mass balance estimates.

5 References

Davison, B. J., Hogg, A. E., Slater, T., & Rigby, R. (2025). Antarctic Ice Sheet grounding line discharge from 1996 through 2023. Earth System Science Data, 1–35. https://doi.org/10.5194/essd-2023-448

Mohr, J.J. & J.P. Merryman Boncori, An Error Prediction Framework for Interferometric SAR Data, IEEE Trans. Geosc. Rem. Sens., Vol 46, pp. 1600-1613, Jun. 2008.

Morlighem, M. (2022). MEaSUREs BedMachine Antarctica. (NSIDC-0756, Version 3). [Data Set]. Boulder, Colorado USA. NASA National Snow and Ice Data Center Distributed Active Archive Center. https://doi.org/10.5067/FPSU0V1MWUB6. [Sep 2025].

Van Wessem, J. M., Reijmer, C. H., Morlighem, M., Mouginot, J., Rignot, E., Medley, B., Joughin, I., Wouters, B., Depoorter, M. A., Bamber, J. L., Lenaerts, J. T. M., Van De Berg, W. J., Van Den Broeke, M. R., & Van Meijgaard, E. (2014). Improved representation of East Antarctic surface mass balance in a regional atmospheric climate model. Journal of Glaciology, 60(222), 761–770. https://doi.org/10.3189/2014jog14j051

Mottram, R., Hansen, N., Kittel, C., Van Wessem, J. M., Agosta, C., Amory, C., Boberg, F., Van De Berg, W. J., Fettweis, X., Gossart, A., Van Lipzig, N. P. M., Van Meijgaard, E., Orr, A., Phillips, T., Webster, S., Simonsen, S. B., & Souverijns, N. (2021b). What is the surface mass balance of Antarctica? An intercomparison of regional climate model estimates. *the Cryosphere*, *15*(8), 3751–3784. https://doi.org/10.5194/tc-15-3751-2021

Shepherd, A., Gilbert, L., Muir, A. S., Konrad, H., McMillan, M., Slater, T., et al. (2019). Trends in Antarctic Ice Sheet Elevation and Mass. Geophysical Research Letters, 46(14), 8174–8183. https://doi.org/10.1029/2019GL082182